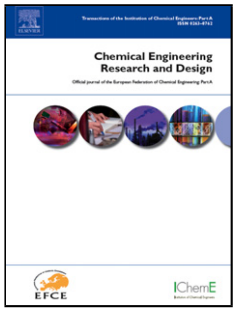

Title: On the Use of 3D-Printed Flow Distributors to Control Particle Movement in a Fluidized Bed

Authors: Akinlolu Oyekunle Oluseun Odeleye, Chih-Yao Chui, Linh Nguyen, Alfonso A. Castrejon-Pita, Hua Ye, Zhanfeng Cui

PII: S0263-8762(18)30522-7
DOI: https://doi.org/10.1016/j.cherd.2018.09.042
Reference: CHERD 3370

To appear in:

Received date: 28-3-2018
Revised date: 19-9-2018
Accepted date: 30-9-2018

Please cite this article as: Odeleye, Akinlolu Oyekunle Oluseun, Chui, Chih-Yao, Nguyen, Linh, Castrejon-Pita, Alfonso A., Ye, Hua, Cui, Zhanfeng, On the Use of 3D-Printed Flow Distributors to Control Particle Movement in a Fluidized Bed.Chemical Engineering Research and Design https://doi.org/10.1016/j.cherd.2018.09.042

On the Use of 3D-Printed Flow Distributors to Control Particle Movement in a Fluidized Bed

Authors

Akinlolu Oyekunle Oluseun Odeleye[1]

Chih-Yao Chui[1]

Linh Nguyen[1]

Alfonso A. Castrejon-Pita[2]

Hua Ye[1]

Zhanfeng Cui*[1]

Author Affiliations

1. CRMI Technology Centre, Institute of Biomedical Engineering, Old Road Campus Research Building, University of Oxford, Oxford, OX3 7DQ, United Kingdom.
2. Department of Engineering Science, Thom Building, Parks Road, University of Oxford, Oxford, OX1 3PJ, United Kingdom.

*Corresponding Author

Name: Professor & Director Zhanfeng Cui

Address: CRMI Technology Centre, Institute of Biomedical Engineering, Old Road Campus Research Building, University of Oxford, Oxford, OX3 7DQ, United Kingdom.

Email: Zhanfeng.Cui@eng.ox.ac.uk

Tel: + 44 (0) 1865 617915

Highlights

- Additive manufacturing can be used to manipulate multiphase flows
- Transition to swirling flow characterized by particle acceleration and deceleration
- Swirling fluidization attained bed heights up to 52% greater than non-swirling
- Particle-wall interactions begin to dominate at high angular fluid velocities
- Bi-directional flow channels enhance the spatial uniformity of radial particle flux

Abstract

3D-printing has emerged as a revolutionary tool for the rapid-prototyping of both conventional and novel products. Its use can foster innovative solutions to engineering challenges that previously would have been considered impractical. We propose the manipulation and control of multiphase systems (e.g. fluidized bed bioreactors) as one such use. The article presented investigates the particle flow and mixing within a fluidized bed induced by novel additive manufactured flow distributors. The fluidized bed is designed for adherent cell expansion on 3 mm diameter calcium alginate macrocarriers. Particle tracking was employed to assess the influence of flow channel angle and direction upon the radial flux of the carriers within the vessel. Uni-directional angled (45^{o}) flow channels generated swirling fluidization of the macrocarriers; increasing particle radial velocities by up to 5.2 times (compared to their vertical flow channel counterparts) at a liquid superficial velocity of 0.0047 m/s. Swirling fluidization also generated particle bed heights up to 52% higher than vertical flow channels. Bi-directional flow channels improved the spatial uniformity of particle radial velocity. In addition, the angular flow channels generated axial velocity gradients that facilitate fluctuations in the height of fluidized particles, thus counteracting elutriation. Finally, lower liquid flow rates and interstitial velocities were required to mix the particles, thus leading to lower hydrodynamic stresses introduced into the

system. The introduction of multi-directional flow channels provides novel options to the design and use of flow distributor technology. We foresee additional advancements in chemical engineering product design utilizing additive manufacturing to manipulate multiphase flows.

Keywords: **3D-Printing. Fluidized Bed, Multiphase Flow, Bioreactor, Swirling Fluidization, Flow Distributor, Angled Flow Channels**

Nomenclature

Roman Characters

d_p Particle diameter, m

n Sample size of tracked particle velocities

r Particle radial position on vessel cross-sectional plane, m

R Radius of fluidized bed cross-section, m

Re_p Particle Reynolds number $\left(Re = \frac{\rho_f d_p |u_f - u_p|}{\mu}\right)$

u_f Liquid superficial velocity, m/s

u_p Particle velocity, m/s

U_i Velocity magnitude of individual tracked particle $\left(U_i = \sqrt{{U_x}^2 + {U_y}^2}\right)$, m/s

$\overline{U}$ Ensembled-average velocity of all tracked particles in dataset, m/s

V_{FCE} Liquid velocity exiting channels of the flow distributor, m/s

Greek characters

μ Liquid viscosity, kg/ms

v_f Liquid kinematic viscosity, m2/s

ρ_p Particle density, kg/m^3

ρ_f Carrier fluid (liquid water) density, kg/m^3

σ Standard deviation, m/s

τ_p Particle relaxation time, s

1. Introduction

The formation and use of multiphase flow is present in a number of industrial applications, from power generation, to the pharmaceutical, biotechnologies and food industries. The control and understanding of multiphase flows is paramount for industries such as the fine chemicals/catalysts sector, which alone is worth over £75 billion/year to the UK economy (Matar, 2015). Many of the applications that possess liquid-solid multiphase flows exhibit solids with a significant distribution of sizes, densities and shapes: Properties that can have an important influence on the flow and mixing of the solid phase.

Fluidized beds in particular are used in a variety of manufacturing processes including food, chemical, petrochemical, pharmaceutical and crystallisation among others (Carlos and Richardson, 1968; Fan, 1996; Jain et al., 2017). The mass and heat transfer characteristics associated with solids fluidization using a fluid "carrier" phase, facilitates its application as a reactor, a fluidized bed combustion system, solids coating, and fluid catalytic cracking, among others.

In the bioprocess industry, fluidized bed bioreactors have been utilised for the growth of adherent cells upon porous macrocarriers (Warnock and Al-Rubeai, 2006), however, their commercial use in the production of cell therapies is limited. Fluidized beds do not suffer from the high localised shear stresses present in mechanically stirred bioreactors such as stirred tanks, due to the carrier-induced mixing (Andrews, 1988). Furthermore, the high mass transfer interface, generated by the

moving liquid and solids, engenders enhanced mass transfer characteristics compared to other mixing systems (Preissmann et al., 1997; Warnock and Al-Rubeai, 2006). The limited radial dispersion of solids observed within fluidized bed bioreactors is well known, with studies suggesting that radial particle dispersion coefficient are lower by an order magnitude, than their axial counterparts (Gabor, 1964; Shi and Fan, 1984).

In order to enhance mixing of solids in the horizontal plane, studies have looked at introducing a tangential flow to the vertical flow to induce a swirling motion (Li et al., 2010), whilst Ouyang and Levenspiel (1986) used a series of overlapping plates shaped as sectors of a circle to fabricate a spiral distributor that allows an angular inlet of flow. The swirling fluidization technique facilitates a reduction in pressure drop required to expand the bed of particles (Miin et al., 2015; Ouyang and Levenspiel, 1986), which, from a bioreactor design perspective, reduces the pumping (and hence power requirements) in addition to the lower interstitial velocities experienced by cells immobilised on the solid phase. Recent Particle Tracking/Image Velocimetry investigations have been performed on fluidized beds incorporating these spiral distributors (Naz and Sulaiman, 2016; Sulaiman et al., 2016). The studies note a Gaussian distribution of velocity along the radial line and an increase in particle velocity as the inclination angle was increased from the horizontal plane. These spiral distributors do not enable swirling fluidization to be induced in the central half of the vessel, due to the arrangement of the overlapping sections. In addition, the ability to utilise particles smaller than 6 mm in diameter was precluded at higher inclination angles due to the potential weeping of particles below the distributor. Typical swirling fluidized beds also possess limitations regarding the ability to introduce angular flow in multiple directions.

With the establishment of 3D-printing as a cost-effective manufacturing strategy, the ability to fabricate complex geometries can aid the development of novel flow distributors, to mitigate

against the limited radial mixing associated with many existing fluidized beds. The production of flow distributors with angular flow channels using traditional (i.e. machining) or other non-additive manufacturing methods, is indeed possible. However, the time and costs associated with using non-additive manufacturing methods, has precluded the widespread fabrication/development of complex geometries within flow distributors (such as those presented herein). Furthermore, additive manufacturing can facilitate even greater geometric complexity (not achievable through traditional methods), to manipulate and control multiphase flows. The aim of this study is to investigate the solids mixing generated by the directional orientation and arrangement of flow channels within flow distributor designs. The primary purpose of the flow distributor is to effectively and uniformly distribute non-porous macrocarriers made of calcium alginate for adherent cell attachment in a fluidized bioreactor. Particle tracking was used to assess the influence of flow channel angle and direction upon calcium alginate bead velocity and spatial characteristics, for application within a bioreactor for stem cell expansion.

2. Materials and Methods

2.1 3D-Printed Flow Distributors

The 3D-printed flow distributors were first designed using Autodesk Inventor (California, USA) computer-aided design software (CAD). The distributors were all 0.1 m in diameter and 0.01 m in thickness. The flow channels for each design were positioned to be equidistant from adjacent flow channels by a distance of 4 mm, both radially and circumferentially. In total, each flow distributor possesses 490 flow channels. Figure 1 illustrates wireframe images of flow channels orientated at different angles offset from the vertical plane a) 0^o (i.e. traditional) b) 45^o (uni-directional or "swirling") and c) 30^o (bi-directional or "counter-swirling"). Flow distributors featuring 0^o, 15^o, 30^o, 45^o (uni-directional) and 30^o (bi-directional) flow channels were designed and 3D-printed

using a Formlabs (Massachusetts, USA) Form 2 3D-printer (using stereolithography technology) at a vertical resolution of 50 µm and horizontal spot size of 140 µm. The components were printed using the Clear FLGPLC02 resin, washed twice with ethanol for 10 mins and post-cured according to the manufacturer's instructions. The flow distributors were also printed using a Makerbot 3D-printer (fused deposition modelling technology) using a 50% infill, polylactic acid resin and a vertical resolution of 200 µm. There was negligible difference in particle bed fluidization noted using both 3D-printing technologies. Which is important from a manufacturing perspective, given the range in costs associated with the variety of additive manufacturing methods commercially available.

The uni-axial angular flow designs were developed to introduce effective radial flux of the macrocarriers, as well as variation in axial fluid velocity to reduce the influence of elutriation (particle segregation by size) on particle mixing. The bi-axial flow channel configuration was developed to augment the random nature of particle and fluid movement (to increase uniformity of cell, macrocarrier and nutrient distribution), while maintaining the benefits of swirling fluidization.

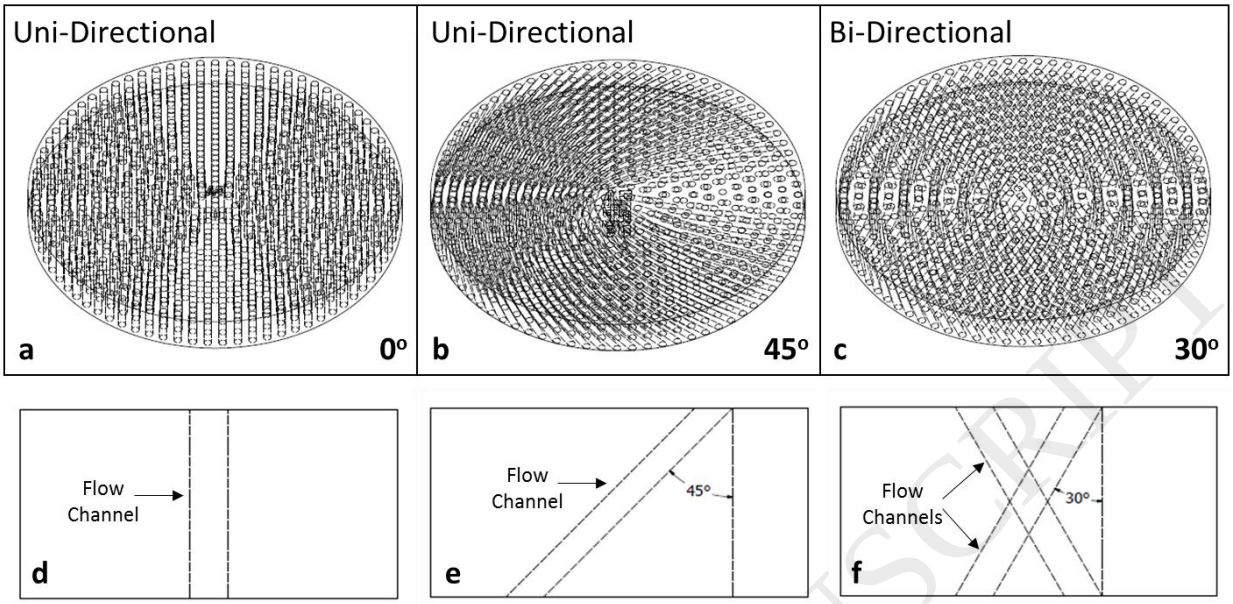

Figure 1: Wireframe drawings of 3D-printed flow distributors and corresponding close-up of individual flow channels: (a and d) uni-directional 0° angled pores; (b and e) uni-directional 45° angled pores and (c and f) bi-directional 30° angled pores.

2.2 Particle Tracking Video Acquisition Set-Up

The calcium alginate beads under fluidization were tracked by video acquisition. A diagram of the experimental set-up for the particle tracking video acquisitions is shown in Figure 2. The set-up includes the fluidized bed, constructed from Perspex: The vessel is composed of a plenum (to homogenise the inlet flow), a column to house the beads and a flow distributor. The cylindrical vessel has an inner diameter of 0.1 m, a plenum height of 0.045 m, a column height of 0.175 and a total height of 0.247 m. Two thread-to-hose barb adaptors were fitted on the bottom and top of the vessel for the inlet and outlet tubing respectively. An Ismatec Ecoline pump (Apeldoorn, Netherlands) was used to pump the fluidizing liquid (in this case de-ionised water) to the bed of macrocarriers. An EOS 100D Canon digital single-lens reflex (SLR) camera, with an 18 megapixel

CMOS and a frame rate of 25 frames per second was attached to a clamp and positioned 1 cm from the vessel head-plate. Tygon® tubing (8 mm ID and 1.6 mm thickness) was attached to the inlet and outlet ports of the fluidized bed and connected to a 2 L bottle to establish the liquid circulatory loop. The fluid inlet line was fed into the pump and the reservoir filled with de-ionised (DI) water. The plenum chamber of the fluidized bed was filled with 250 mL of 6 mm diameter acrylonitrile butadiene styrene beads (ABS), to aid in the homogenisation of the in-coming fluid. The fluid was then pumped up through the vessel to mix and fluidize the bed of calcium alginate beads.

The calcium alginate beads were prepared by electrospraying a 2% alginate solution into a beaker of calcium chloride. The beads were measured to be 3.014 mm (s.d. 0.068) in diameter with a density of 1.08 g/cm^3 (measured from 100 mL of calcium alginate beads). Calcium alginate beads are naturally white/translucent, so a portion of beads were prepared with black colouring to facilitate particle tracking in later image processing steps. 95 mL of white/translucent beads were prepared for the fluidized bed, and 15 black coloured beads were added to the 95 mL bead bed. A video acquisition of the fluidized particles was acquired at a rate of 25 frames per second, for a minimum of 10 seconds. The videos were then saved for post-processing particle tracking.

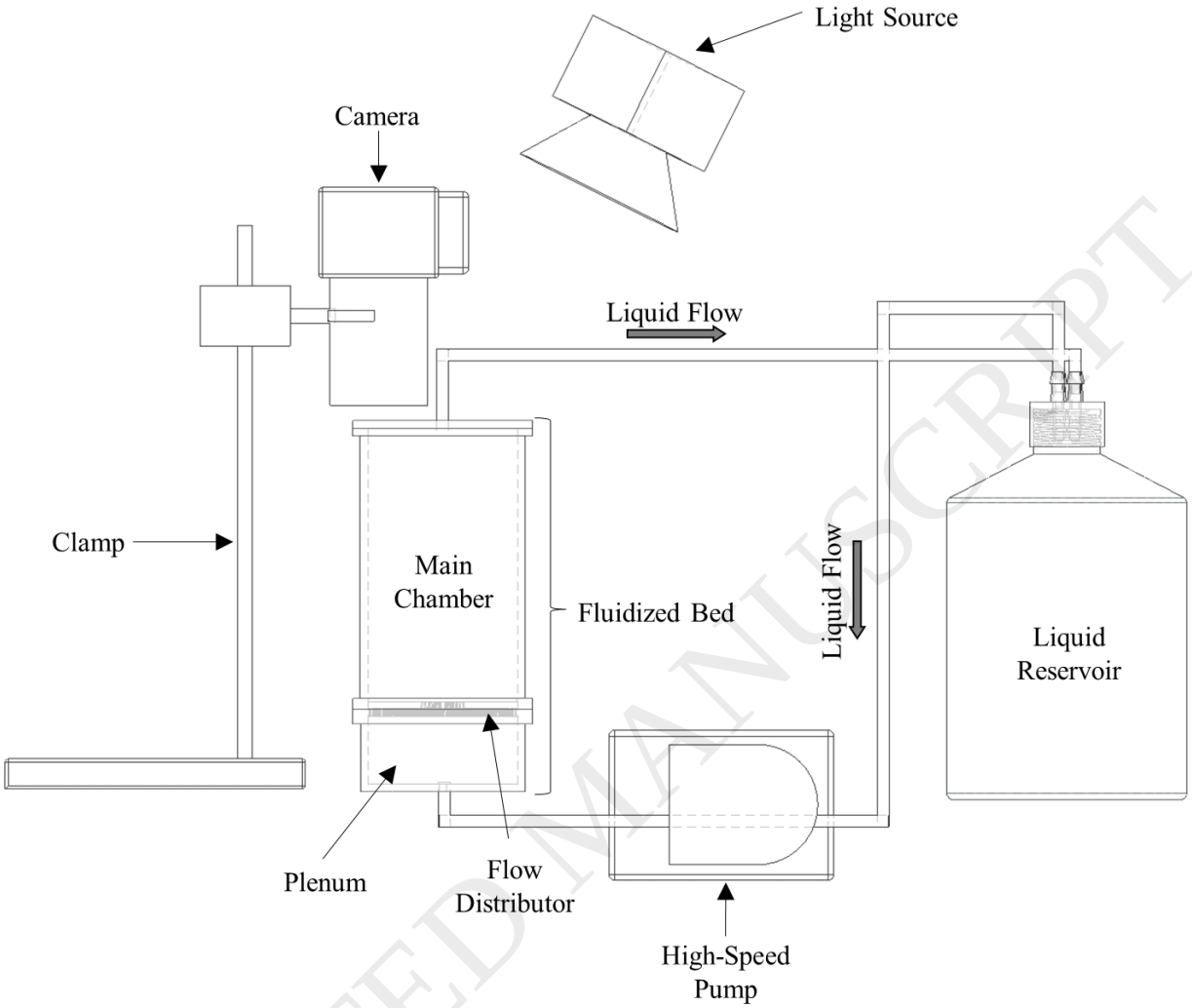

Figure 2: Schematic diagram of particle tracking video acquisition experimental set-up.

2.3 Particle Tracking Image Processing

The particle movement was assessed for superficial liquid velocities of 3.1, 3.9, 4.7, 5.5, 6.3 and 7.1 mm/s, corresponding to 40%, 50%, 60%, 70%, 80% and 90% of the pumps capacity, respectively. These superficial velocities are obtained from the vessel cross-sectional area; the corresponding flow channel exit velocities are 0.016, 0.020, 0.024, 0.028, 0.032, 0.036 m/s, respectively. Once the videos were acquired and saved, they were processed using MATLAB. The videos were decomposed into individual frames, at 0.08 second time increments. Figure 3 summarises the steps performed during the particle tracking algorithm. The images were converted

from colour to grayscale (Fig. 3a) using a weighted average of the three colour channels i.e. 0.299, 0.587 and 0.114 for red, green and blue channels respectively. The grayscale image pixel values were inverted (to convert the black beads to white) as shown in Fig. 3b, before applying a Laplacian of Gaussian filter to further highlight the coloured beads whilst reducing the amount of background noise within the image (Fig. 3c). This pre-processing step also results in a slight reduction in the size of the particles. Particle tracking algorithms were adapted from open source code banks (Blair and Dufresne, 2008). The tracking algorithm was first used to locate the particles by assuming that local maxima in pixel intensity corresponded to a particle to be tracked. A size criterion of 20x20 pixel kernels (image resolution of 0.1 mm/pixel) and a peak value of 0.6 (in a binary image of 0 to 1) was selected in order to ensure that only objects of a particular size and focal plane was tracked. However, given the tidal form of the particles in wave motion, a precise determination of the vertical height of each particle throughout its path was not achievable under the experimental conditions used. Each pixel above a set threshold was investigated to assess if it was brighter than its neighbours. The peaks within a specified size range from each other were compared to select and keep the brightest peak. The co-ordinates of the centroids corresponding to each peak were then obtained and a tracking algorithm applied to identify particles in consecutive images that had moved within 30 pixels of each other. The tracked particles were tagged and collated into a table of particle identification numbers and their corresponding location in space and time.

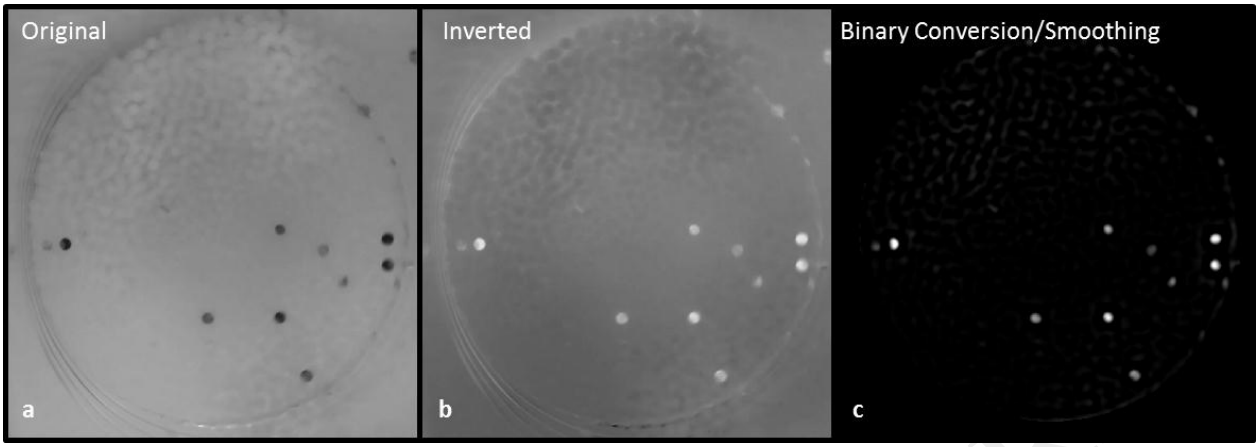

Figure 3: Image processing steps for particle identification showing: a) raw particle image in grayscale; b) inverted particle image and c) binary conversion (post smoothing via Laplacian of Gaussian).

2.4 Particle Tracking Statistical Analysis

Figure 4 illustrates the individual data points of a series of tracked particles with a flow channel liquid exit velocity of 0.036 m/s, using a swirling flow distributor at 15^{o}. The velocities of the tracked particles under swirling flow, fluctuate between periods of acceleration and deceleration, whilst individual velocity data points lay within a fixed range of 0 to 0.032 m/s.

The cumulative moving average (CMA), calculated using Equation 1, enables an assessment of the sample size of tracked particles required to generate an ensemble-averaged particle velocity of minimal standard error.

$$\mathrm{CMA}_n = \frac{x_1 + \cdots + x_n}{n} \quad (1)$$

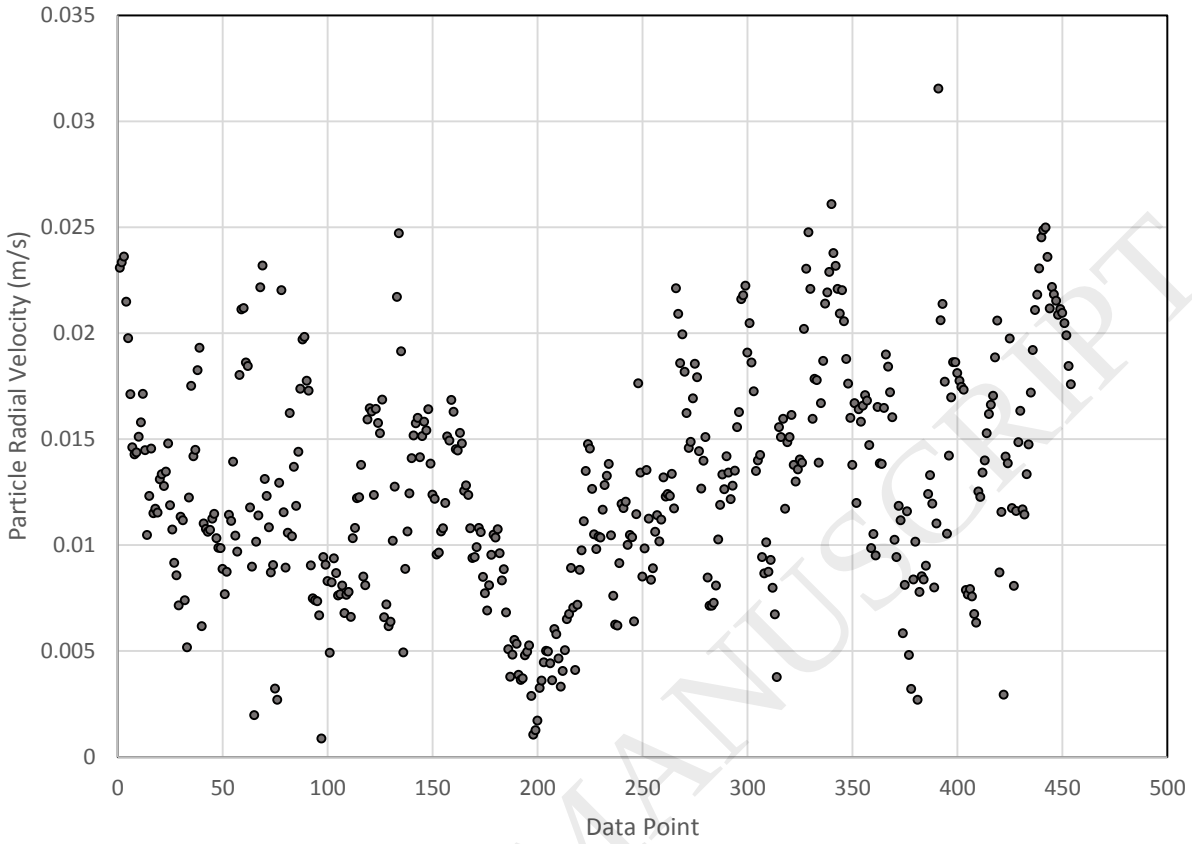

Figure 4: a) Plot of tracked particle velocities at a flow channel exit velocity of 0.036 m/s, using uni-directional flow channel angles of 15º.

Figure 5 displays cumulative moving average of particle velocity, with respect to the number of tracked particle velocities, for data obtained at flow channel exit velocity of 0.02 m/s, using uni-directional flow channels of 0º, 15º, 30º and 45º. Convergence of the CMA profile to the population average occurs within 200 data points for each of the conditions presented. The standard error (as calculated using Equation 2 (Oliveira et al., 2015; Shokri et al., 2017)) for the mean velocity from 200 data points was 0.00012, 0.00015, 0.00025 and 0.00042 m/s at flow channel angles of 0º, 15º, 30º and 45º, respectively.

$$\mathrm{SE} = \sqrt{\frac{\sum_{i=1}^{n}(U_i - \bar{U})^2}{n(n-1)}} \qquad (2)$$

The greater uncertainty (as calculated using Equation 2) observed at the shallower flow channel angles, can be explained by an increased two-way coupling of particle and liquid momentum transfer at greater radial particle velocities.

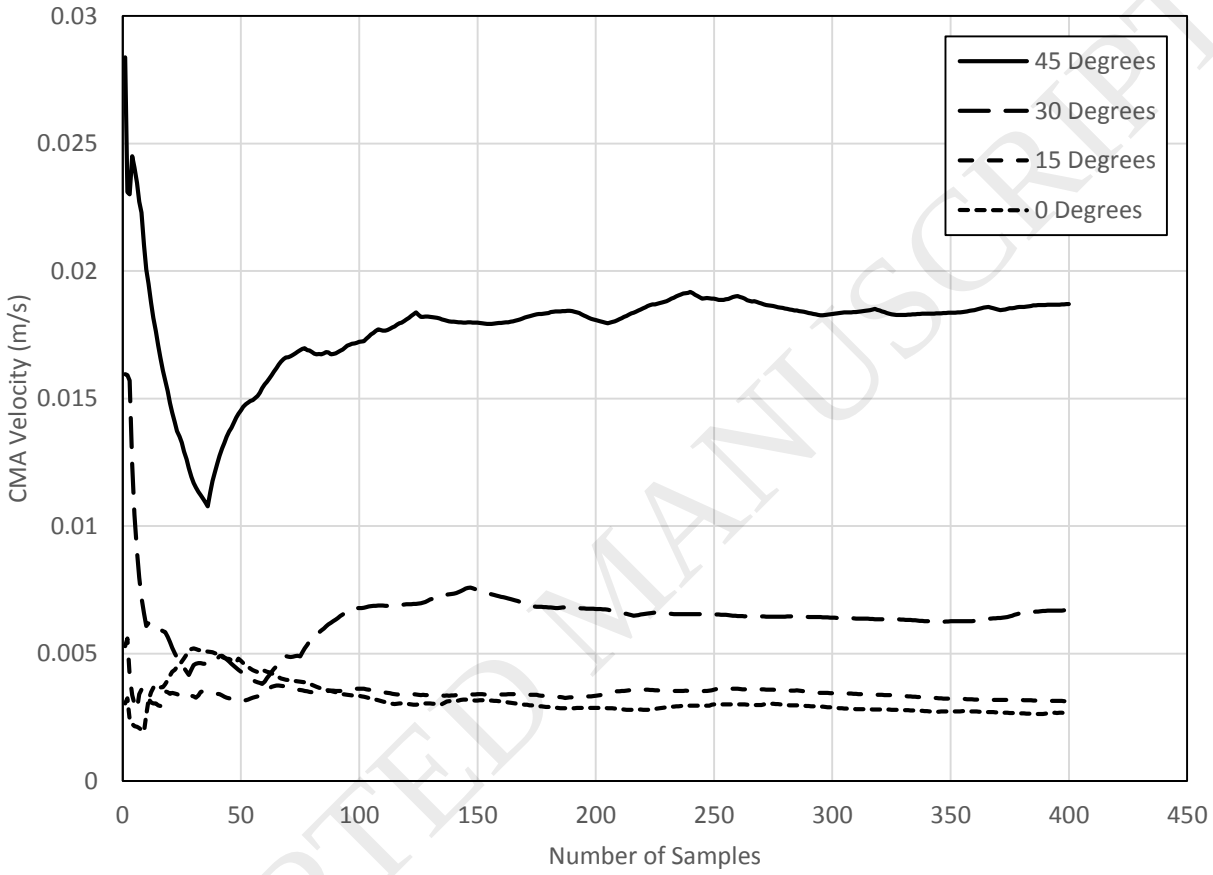

Figure 5: a) Plot of cumulative moving average of radial particle velocity at a flow channel exit velocity of 0.020 m/s, using uni-directional flow channels of 0º, 15º, 30º and 45º.

3. Results and Discussion

3.1 Particle Motion

Particle motion in the radial plane is pertinent in many fluidized bed applications. Figure 6 shows the centroid locations of tracked particles under fluidization after a period of 10 seconds, at a flow channel exit velocity of 0.036 m/s, for flow distributors with a) 0^o uni-directional, b) 45^o uni-

directional and c) 30° bi-directional flow channels. Figure 6a illustrates the significantly lower radial movement of particles using the traditional vertical flow distributor design. Under swirling fluidization (Fig. 6b), the particles travel in an orbital pattern akin to a rotational vortex. The flow within a rotational vortex rotates like a rigid body i.e. the orbital speed at the perimeter is the same as that close to the centre. Thus given the larger orbital distance close to the perimeter of the vessel, the particle velocities are higher. This is further quantified in Figure 10, which displays particle velocity with respect to radial distance from the vessel centre-point. Figure 6c shows a uniquely random movement of particles with a variety of patterns traversing the cross-section of the vessel. The random nature of the particle movement leads to increased particle collisions and hence lower particle velocities than under swirling flow. The uni-directional movement of particles is also likely to contribute to greater velocities under swirling flow, which would be explained by greater conservation of momentum under swirling flow

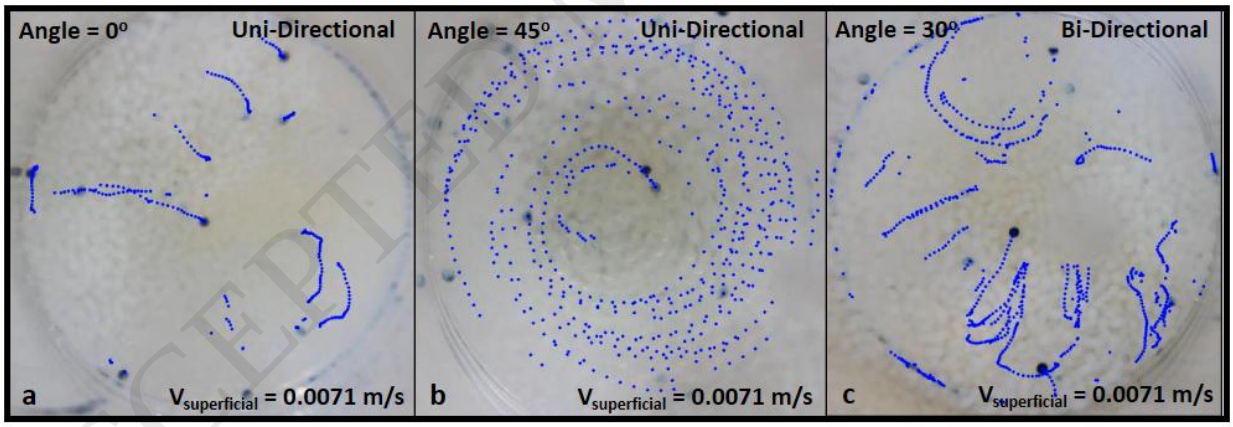

Figure 6: Top-down view of fluidized bed illustrating particle movement after 10 seconds of fluidisation, using: a) Traditional at 0^{o} and V_{FCE} = 0.036 m/s; b) swirling 45^{o} and V_{FCE} = 0.036 m/s and c) counter-swirling at 30^{o} and V_{FCE} = 0.036 m/s.

Figure 7 shows the variation in ensemble-averaged particle velocity with respect to the liquid flow rate (or flow channel exit velocity), using flow channels at 0°, 15°, 30° and 45° from the vertical plane. The profiles for each of the designs exhibit a similar shape of linearly increasing velocity

from V_{FCE} = 0.016 to 0.028 m/s, that reaches a plateau, occurring from V_{FCE} = 0.028 to 0.036 m/s. In the case of 0°, the particles fluidized at V_{FCE} = 0.028 to 0.036 m/s exhibit a fully turbulent regime. For beads fluidized under a swirling regime, the plateau in particle velocity commences sooner at angles of 45° compared to the other designs. This observation can be explained by greater wall interactions under swirling flow at V_{FCE} velocities of more than 0.028 m/s: As the higher velocity liquid exits the angled flow channels, it pushes the beads closer to the perimeter of the vessel.

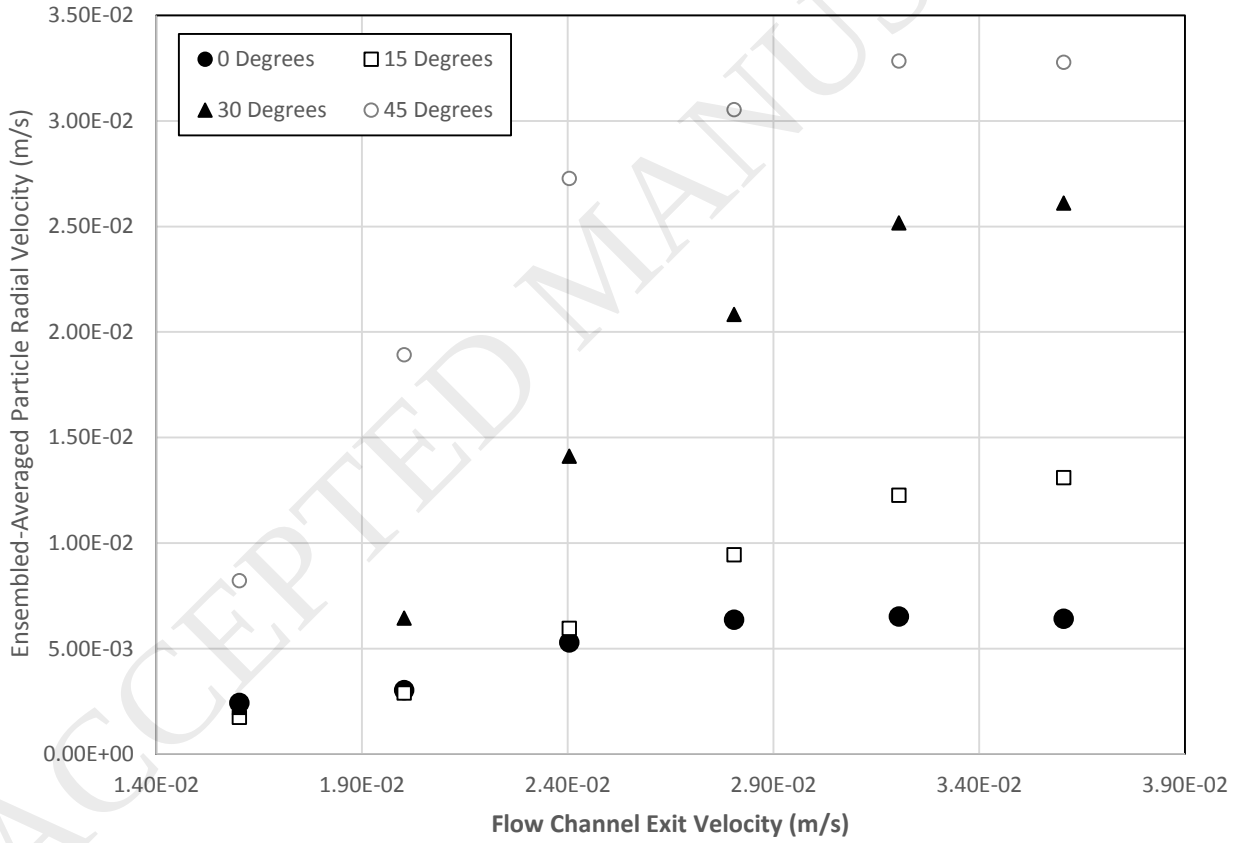

Figure 7: Plot of ensemble-averaged particle velocity vs V_{FCE}.

The increasing flow channel angles also induce both swirling movement of the beads and bed expansion at lower liquid flow rates. This is particularly the case at 45°, where radial velocities of

0.0082 m/s are measured at V_{FCE} = 0.016 m/s, compared to the 0.0017 m/s particle velocity measured at 15°. For pore angles of 0° and 45° (at V_{FCE} = 0.04 m/s), fluidized bed heights of 0.048 m and 0.073 m were noted, respectively. This confirms that a lower liquid velocity is required to fluidize the particle bed at higher flow channels angles. A lower velocity leads to a reduction in pressure drop and, in the context of adherent cell culture, shear forces that can be detrimental to the cells.

3.2 Theoretical Considerations

To mathematically describe the particle-laden flow exhibited in this study, the classical Navier-Stokes equations require modification to take into account the influence of the carrier fluid (in this case water) upon the particles. The particles can be influenced by the carrier and/or vice versa, in addition to the size, density and concentration of the particles. The simplified momentum equation for a particle is:

$$\frac{du_p}{dt} = \frac{1}{\tau_p}\left(u_f - u_p\right) \tag{3}$$

Where u_p and u_f represent the particle and carrier fluid velocity, respectively, and τ_p is the relaxation time of the particle. Parameters such as buoyancy, pressure gradient and added mass were considered negligible for simplicity. The relaxation time represents the time taken for a particle to respond to changes in velocity of the carrier fluid. For particles that are much smaller than the Kolmogorov length scale, the lift forces have been shown to be of the same order of magnitude as the drag forces (Meller and Liberzon, 2015). This is not applicable to the current study given the large size of the beads. According to Burton and Eaton (2005), for a homogenous flow around a fixed particle, the Stokes drag is the dominant term in the particle equation of motion. Whilst the history term, fluid pressure gradient and viscous stress were observed to be

small. This holds true for particles twice the size of the turbulence eddy Kolmogorov scale (Burton and Eaton, 2005). In this study, the drag term is considered the dominant interaction between the fluid and the solid phases. The relaxation time can be estimated using Stokes drag assumption (Brennen, 2005):

$$\tau_p = \frac{\rho_p d_p^2}{18\mu_f} \tag{4}$$

The drag term C_D is a function of the relative particle Reynolds number.

$$Re_p = \frac{\rho_f d_p |u_f - u_p|}{\mu_f} \tag{5}$$

The Oseen correction is used for $Re_p > 1$, and for Re_p of up to 200 the following definition of the relaxation time can be used (Geurts et al., 2007):

$$\tau_p = \frac{\left((2\rho_p + \rho_f)/\rho_p\right) d_p^2}{36 v_f (1 + 0.15 Re^{0.687})} \tag{6}$$

Ensemble-averaged particle Reynolds numbers measured from the tracked particle data were below 100 for the experiments conducted in this study. The relaxation time can also be calculated from the tracked velocity data. The trapezoidal scheme was used to integrate Equation 2 (Ansys, 2003):

$$\frac{u_p^{n+1} - u_p^n}{\Delta t} = \frac{1}{\tau_p}\left(u^* - u_p^*\right) + \cdots \tag{7}$$

Where n is the sequential tracking number for a particle.

$$u^* = \frac{1}{2}(u^n + u^{n+1}) \tag{8}$$

$$u_p^* = \frac{1}{2}(u_p^n + u_p^{n+1}) \quad (9)$$

The particle relaxation represents a timescale of the particle's reaction to changes in the liquid phase velocity. However, localised carrier phase velocity was not obtainable in the experiments conducted. Thus when applying the above equations, the carrier fluid interstitial velocity is kept constant for each liquid flowrate investigated. For this reason, the tracked particle velocity relative to the carrier phase interstitial velocity (in absolute terms) was used when calculating the particle relaxation time, as determined using Equation 7 (conveyed in Equation 10). This allows for the comparison of particle response times between the different flow distributors and flowrates used.

$$\tau_p = \left| \frac{(u^* - u_p^*)}{(u_p^{n+1} - u_p^n)/\Delta t} \right| \quad (10)$$

Figure 8 shows the trend between relaxation time and flow channel angle for flow channel exit velocities of 0.020, 0.028 and 0.036 m/s, using both the Stokes drag-assumed relaxation time and integration of the particle tracking data. As indicated from the results thus far, the particle velocity in the horizontal plane, correlates positively with flow channel angle. Theoretically (as observable in equation 5), when Re_p increases τ_p should decrease. However, under swirling fluidization, expanded bed height is greater (at the same liquid flow rate) as the angles increase. With the expanding bed comes a higher void fraction, which leads to a reduced interstitial (or slip) velocity; thus the Re_p is not directly proportional to the liquid velocity. The slightly higher relaxation times (derived from experimental particle tracking data) noted at angles of 15^o and 30^o, may perhaps be due to the additional particle-fluid interaction forces that were not considered in this study. The particle relaxation time at 15^o (Figure 8a) for both the particle tracking and the drag only theoretical estimation, indicates that the assumption of the drag force being the dominant component of the particle equation of motion holds true at these conditions. However, at increasing fluid velocity

and flow channel angles the particle tracking derived relaxation time increases drastically. This indicates that an additional force is acting upon the particles, which could be the increased particle-wall interactions observed at the higher angles. Thus, the efficiency of momentum transfer from the carrier fluid to the particle reduces as both the flow channel angles and liquid velocity increase.

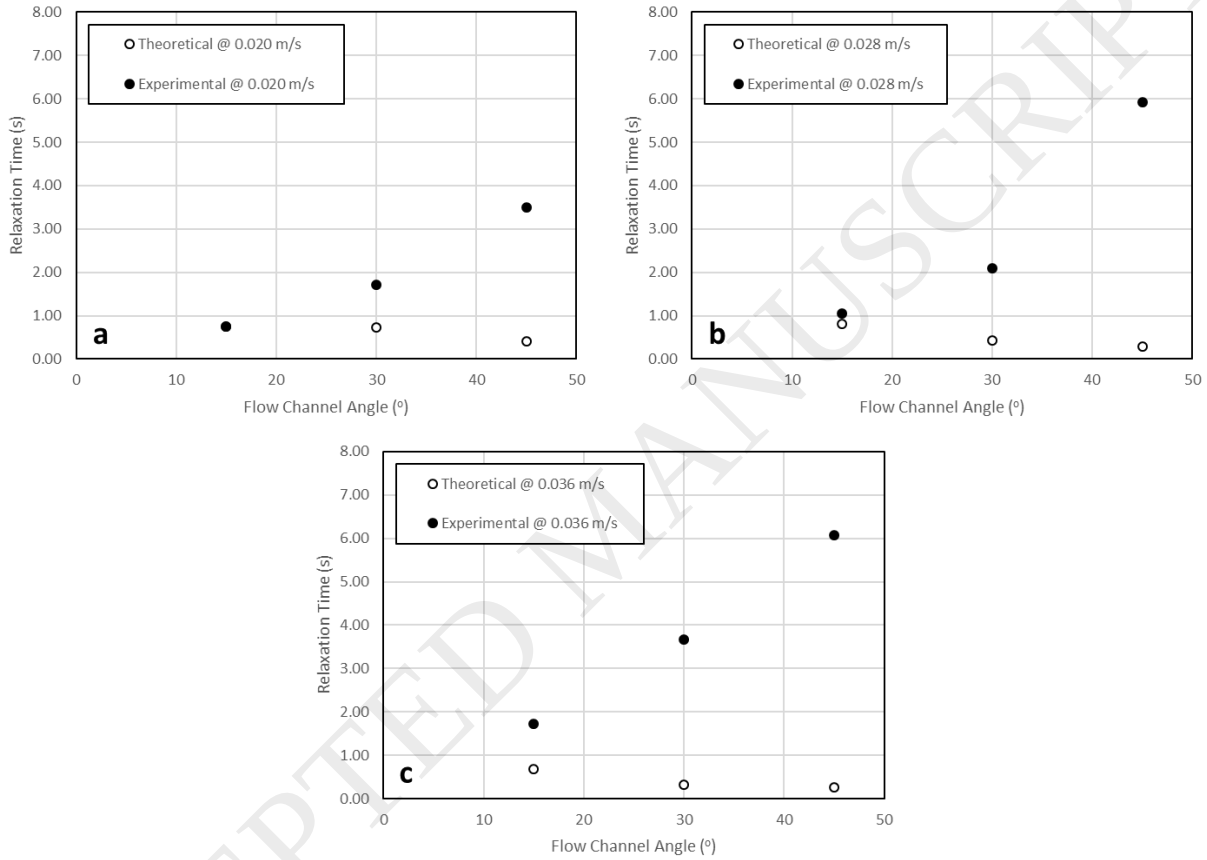

Figure 8: Plot of theoretical and experimentally-derived particle relaxation time (seconds) vs flow channel angle (°) for V_{FCE} at: a) 0.020 m/s; b) 0.028 m/s and c) 0.036 m/s.

3.3 Swirling Flow Transition

To assess the velocity characteristics of the particle-laden flow throughout the transition to swirling flow, a normal probability density function (PDF) was determined using Equation 11:

$$f(x,\mu,\sigma) = \frac{1}{\sqrt{2\pi}\sigma} e^{-\frac{(x-\mu)^2}{2\sigma^2}} \quad (11)$$

Figure 9 displays the PDF of particle velocities tracked at $V_{FlowChannel}$ = 0.020, 0.028 and 0.036 m/s using swirling flow distributors with flow channel angles of 15°, 30° and 45°. The figure conveys three distinct phases of particle velocity distribution, with both liquid flow rate and flow channel angle directly affecting the transition between these phases. Firstly, at low angles and/or flow channel exit velocities i.e. 15° and 0.020 m/s, the velocity distribution is quite narrow. A low ensemble-averaged particle velocity accompanies a commensurately high standard deviation. At these conditions, particle velocity profiles illustrate periods of acceleration and deceleration, indicating that the beads are repeatedly moving into and out of the angled liquid jets induced by the flow channels. As the liquid flow rate and/or flow channel angle increase, the mean particle velocity increases as the PDF becomes broader. In this regime (e.g. 45°, at V_{FCE} = 0.028 and 0.036 m/s) the particles exhibit the same accelerating/decelerating velocity profiles as at lower angles/flow rates, albeit with a relatively broader distribution of velocities (in proportion to the mean particle velocity). The particle acceleration/deceleration noted can be observed in wave type particle motion which was also observed by Sreenivasan and Raghavan (2002). Thirdly, at the highest flow rates and angles tested (0.036 m/s and 45°), a full-bodied particle swirling motion is observed qualitatively. Quantitatively this correlates to an increase in mean velocity but a slight narrowing of the PDF. Although there is still fluctuation in the particle velocities, the sharp periods of acceleration/deceleration are not as profound. Thus, particles are orbiting with a more consistent speed. The particle bed height used in this study is relatively shallow (0.021 m packed bed height), thus the two layered flow regimes observed by Sreenivasan and Raghavan (2002) were not noted in the investigations performed.

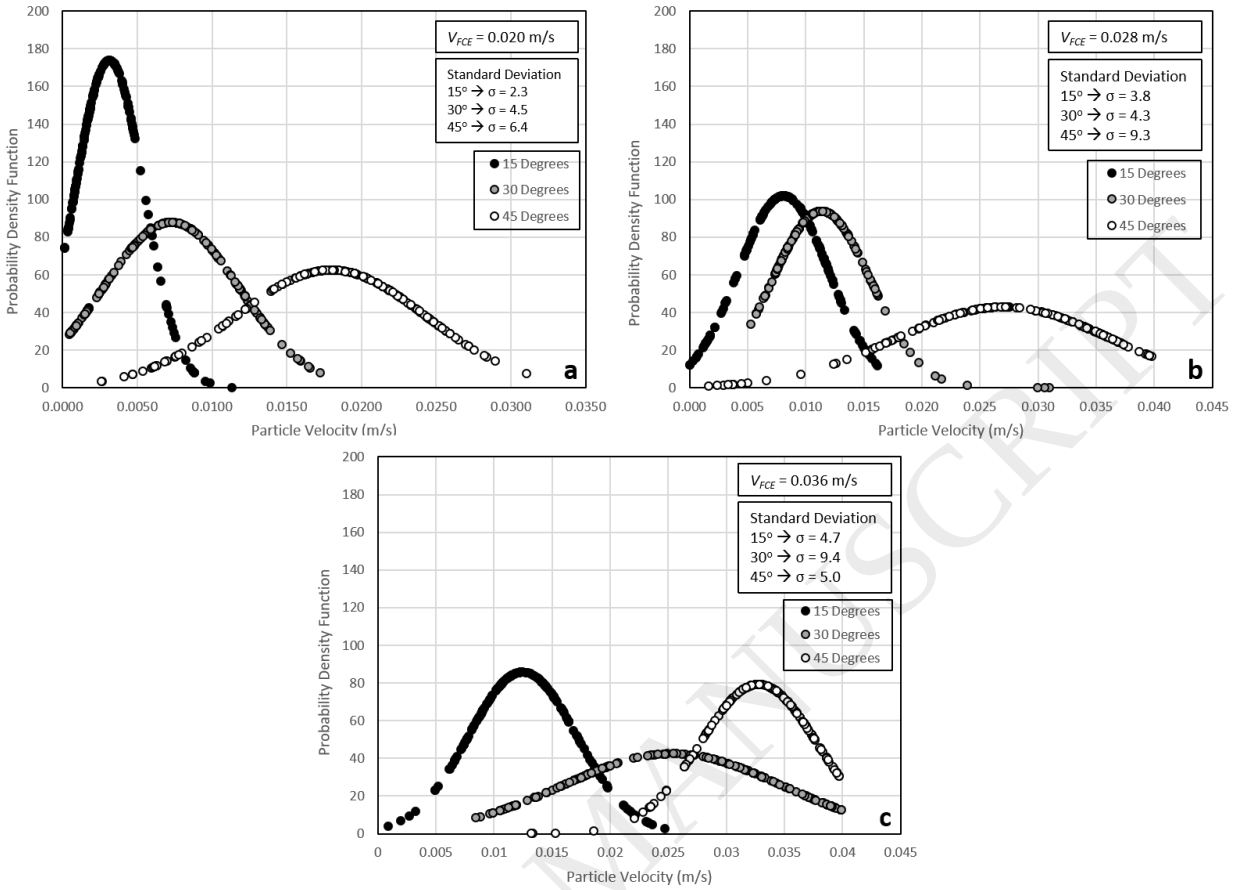

Figure 9: Plot of probability density function of particle velocities at flow channel angles of 15°, 30° and 45°, for flow channel exit velocities: a) 0.020 m/s; b) 0.028 m/s and c) 0.036 m/s.

3.4 Radial Particle Mixing

Although uni-directional angled flow channels can generate ensemble-averaged velocities (under swirling flow) more than 5 times greater than values measured using typical vertical flow channels, the spatial distribution of these velocities is not uniform. The swirling nature of the flow enables prolonged movement of the particles, through conservation of particle momentum. However, this then leads to defined streamlined trajectories of the particles. Thus, when the aim of fluidization is to thoroughly mix the solid phase, greater complexity in the induced flow is required. Figure 10 shows particle velocities with respect to their radial location for flow distributors with uni-directional 30° angle flow channels and bi-directional 30° angle flow channels, both using V_{FCE} =

0.024 m/s. Figure 10a illustrates a low velocity range of between 0.003 and 0.0058 m/s at a radial distance of 0.01 m from the flow distributor centre-point. The velocity range then increases, with greater distance from the centre-point, peaking with 0.0306 m/s at a radial distance of 0.0402 m (radial location r/R = 0.8) from the centre. The velocity range then reduces on approach to the vessel inner wall (0.05 mm from the centre): Again, an indication of the influence of the wall frictional forces on the particle velocities. Figure 10b shows a more uniform spatial distribution of the bead radial velocities compared to the swirl inducing distributor designs, with particle velocities of up to 0.0135 m/s, 0.0152 m/s and 0.0143 m/s at radial locations of r/R = 0.31, 0.62 and 0.94, respectively. Overall, the bi-directional flow channels induce lower particle velocities compared to swirling flow regimes, due to the highly chaotic nature of the mixing generated by the bi-directional flow channels. A significant portion of the particles in this flow regime exhibit velocities of close to zero, which adds further indication to the turbulent nature of the particle mixing. An additional measure to quantify the radial particle mixing efficiency is the total particle migration. The total distance covered by particles after 8 seconds of fluidization (V_{FCE} = 0.024 m/s) using flow channels of 0^o uni-directional, 30^o uni-directional and 30^o bi-directional is measured as 0.30, 0.45 and 0.50 m, respectively. The comparable migration distances between the uni- and bi-directional angled flow channels is due to the greater number of particles tracked under bi-directional fluidization. This occurs because the bi-directional angled flow distributor induces random movement of particles in the axial direction, compared to the more streamlined nature of particle movement under swirling fluidization. To further characterise particle mixing, the mean-square-displacement (MSD) of particles can be used to measure particle dispersion, with the equation show below (Kiared et al., 1997):

$$\text{MSD} = \frac{1}{n}\sum_{i=1}^{P}(X_i - \bar{X})^2 \qquad (12)$$

The MSDs at a liquid superficial velocity of 0.0071 m/s for a bi-directional angled (30^o) flow distributor is 0.36 m and 0.45 m in the x and y-plane, respectively. Whilst the equivalent MSD values using a vertical (0^o) uni-directional flow distributor are 0.36 m and 0.28 m in the x and y-plane, respectively. It is also important to note that only moving particles are tracked to determine the velocities and displacements obtained. Hagemeier et al. (2015) used the number of particles tracked within a given area to determine the local solids volume fraction during particle tracking of a particle-laden flow. In the study presented, the solid volume fraction remains constant for each condition. Therefore, understanding the number of particles tracked also enables an assessment of the relative degree of mixing between the different investigations. The number of tracked particles during 8 seconds of fluidization in both uni-directional vertical (0^o) and bi-directional angled (30^o) flow distributors at a superficial velocity of 0.0071 m/s, was measured at 49 and 99, respectively. Indicating that double the number of particles are in flux using the novel multi-directional flow distributors compared with traditional perforated plates.

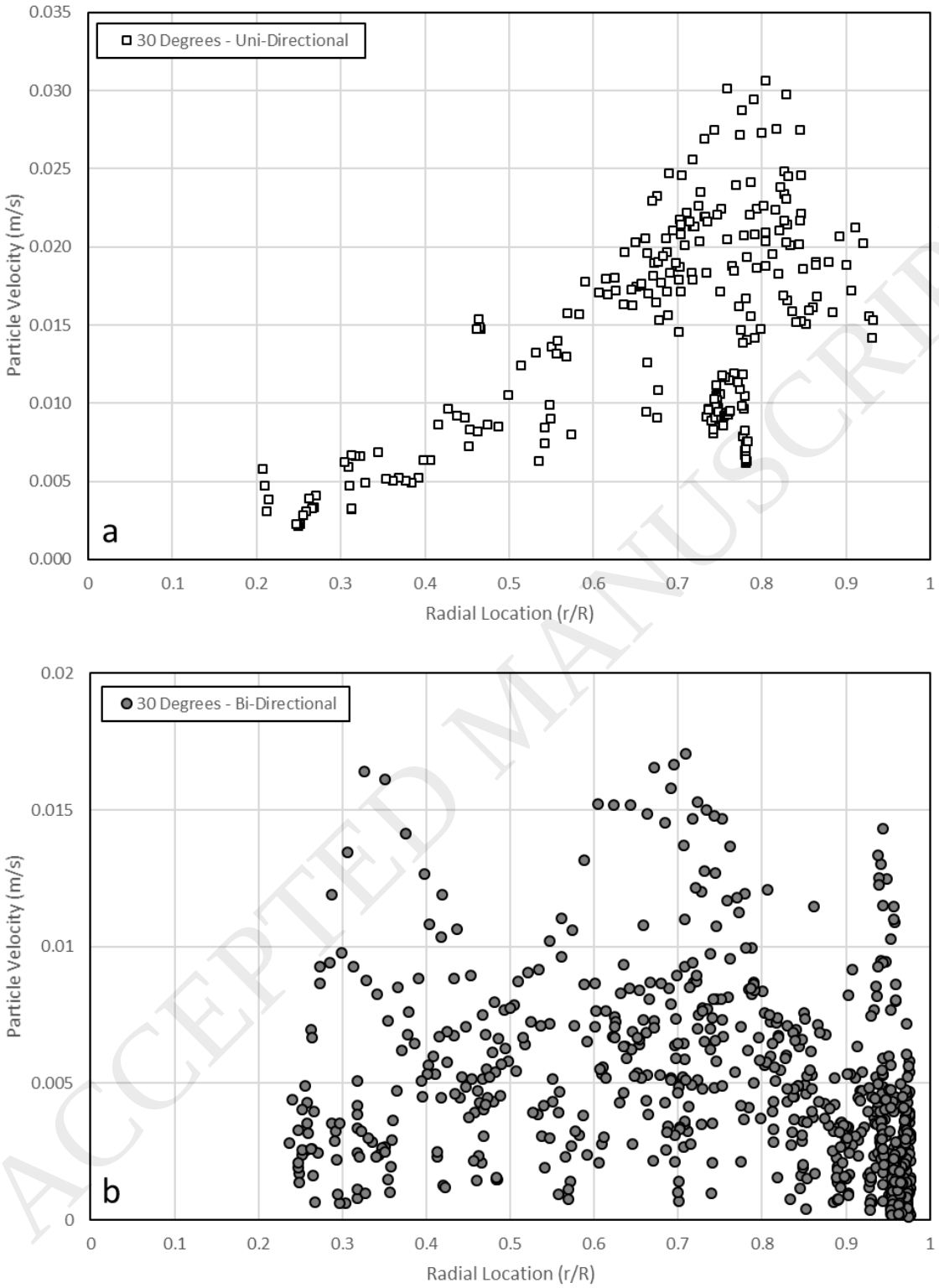

Figure 10: Plot of particle velocity with respect to its radial distance from the vessel centre point, for flow distributors with a) 30° flow channels uni-direction flow channels and b) 30° bi-directional flow channels.

4. Concluding Remarks

The use of fluidization technology for cell therapy manufacturing applications requires careful consideration of the complex flow induced. In addition, the limitations associated with the use of fluidized beds e.g. pressure drop, liquid velocity and macrocarrier mixing, must be optimised to provide the most auspicious environment for the cells as possible. The study presented demonstrates that careful design of the flow channel architecture within 3D-printed flow distributors can be used to generate complex mixing regimes. The swirling flow distributors generated particle radial velocities up to 6 times greater than their non-swirling counterpart. Furthermore, the swirling fluidization facilitated a greater expansion in bed height, which also led to a reduced particle Reynolds number. Bi-directional angled flow distributors provided even greater unpredictability to the particle movement, which is a desirable feature from a bioreactor operation perspective, with uniformity in cell and carrier distribution a key parameter during cell culture. A note must be made of the increased particle-wall interaction that occurs during swirling fluidization at high flow rates. At low flowrates and flow channel angles, the drag forces dominate the particle flux. However, at 45^{o} with V_{FCE} from 0.028 m/s upwards, particle-wall interaction becomes a key parameter. Therefore, the optimal flow rates for a given system should consider these limitations. Nevertheless, the flexibility and precision of 3D-printing can be utilised to tailor the flow in a variety of systems.

To further optimise the developed designs, computational fluid dynamics is a clear next step. Experimental studies as described in this article are imperative to the development and validation of such models. The use of additive manufactured angular flow distributors can play a key role not only in bioreactor technology, but in the various industrial chemical technologies in which fluidized bed, mixing and liquid-solid control are prevalent and required.

Acknowledgements

This research was supported through funding from China Regenerative Medicine International Limited (CRMI) [grant numbers DFR00150].

References

Andrews, G., 1988. Fluidized-bed bioreactors. Biotechnol. Genet. Eng. Rev. 6, 151–178.

Ansys, 2003. Fluent 6.1. User's Guide.

Blair, D., Dufresne, E., 2008. The Matlab Particle Tracking Code Repository [WWW Document]. Matlab Part. Track. URL http://physics.georgetown.edu/matlab/ (accessed 7.12.16).

Brennen, C., 2005. Fundamentals of Multiphase Flows. Cambridge Univ. Press 128, 36.

Burton, T.M., Eaton, J.K., 2005. Fully resolved simulations of particle-turbulence interaction. J. Fluid Mech. 545, 67.

Carlos, C.R., Richardson, J.F., 1968. Solids movement in liquid fluidised beds—I Particle velocity distribution. Chem. Eng. Sci. 23, 813–824.

Fan, L.S., 1996. Summary paper on fluidization and transport phenomena. Powder Technol. 88, 245–253.

Gabor, I.D., 1964. Lateral solids mixing in fludized-packed beds. AIChE J. 10, 345–350.

Geurts, B.J., Clercx, H., Uijttewaal, W., 2007. Particle Laden Flow. Springer Netherlands, Enschede, Eindhoven, Delft.

Hagemeier, T., Roloff, C., Bück, A., Tsotsas, E., 2015. Estimation of particle dynamics in 2-D fluidized beds using particle tracking velocimetry. Particuology 22, 39–51.

Jain, V., Kalo, L., Kumar, D., Pant, H.J., Upadhyay, R.K., 2017. Experimental and numerical investigation of liquid–solid binary fluidized beds: Radioactive particle tracking technique and dense discrete phase model simulations. Particuology.

Kiared, K., Larachi, F., Cassanello, M., Chaouki, J., 1997. Flow Structure of the Solids in a Three-Dimensional Liquid Fluidized Bed. Ind. Eng. Chem. Res. 36, 4695–4704.

Li, F., Briens, C., Berruti, F., McMillan, J., 2010. Penetration of High Velocity Horizontal Gas Jets into a Fluidized Bed at High Temperature, in: The 13th International Conference on Fluidization - New Paradigm in Fluidization Engineering. pp. 1–8.

Matar, O., 2015. No more empirical correlations. TCE Chem. Eng. 42–45.

Meller, Y., Liberzon, A., 2015. Particle-fluid interaction forces as the source of acceleration PDF invariance in particle size, International Journal of Multiphase Flow.

Miin, C.S., Sulaiman, S.A., Raghavan, V.R., Heikal, M.R., Naz, M.Y., 2015. Hydrodynamics of multi-sized particles in stable regime of a swirling bed. Korean J. Chem. Eng. 32, 2361–2367.

Naz, M.Y., Sulaiman, S.A., 2016. PTV profiling of particles motion from the top and side of a swirling fluidized bed. J. Instrum. 05019, 11.

Oliveira, J.L.G., Van der Geld, C.W.M., Kuerten, J.G.M., 2015. Lagrangian velocity and acceleration statistics of fluid and inertial particles measured in pipe flow with 3D particle tracking velocimetry. Int. J. Multiph. Flow 73, 97–107.

Ouyang, F., Levenspiel, O., 1986. Spiral Distributor for Fluidized Beds. Ind. Eng. Chem. Process Des. Dev. 25, 504–507.

Preissmann, A., Wiesmann, R., Buchholz, R., Werner, R.G., Noé, W., 1997. Investigations on oxygen limitations of adherent cells growing on macroporous micro-carriers. Cytotechnology 24, 121–134.

Shi, Y.-F., Fan, L.T., 1984. No Title, in: Ind. Eng. Chem Proc. Dev. p. 337.

Shokri, R., Ghaemi, S., Nobes, D.S., Sanders, R.S., 2017. Investigation of particle-laden turbulent pipe flow at high-Reynolds-number using particle image/tracking velocimetry (PIV/PTV). Int. J. Multiph. Flow 89, 136–149.

Sreenivasan, B., Raghavan, V.R., 2002. Hydrodynamics of a swirling fluidised bed. Chem. Eng. Process. 41, 99–106.

Sulaiman, S.A., Miin, C.S., Naz, M.Y., Raghavan, V.R., 2016. Particle Image Velocimetry of a Swirling Fluidized Bed at Different Blade Angles. Chem. Eng. Technol. 39, 1151–1160.

Warnock, J.N., Al-Rubeai, M., 2006. Bioreactor systems for the production of biopharmaceuticals from animal cells. Biotechnol. Appl. Biochem. 45, 1–12.